Journal of Sound and Vibration (1998) **213**(5), 843–863

THE HIGH-FREQUENCY RESPONSE OF A PLATE CARRYING A CONCENTRATED MASS/SPRING SYSTEM

E. H. Dowell and D. Tang

Duke University, Durham, NC 27708-0300, *U.S.A.*

(*Received* 22 *November* 1996, *and in final form* 15 *January* 1998)

The high-frequency response of a plate carrying a concentrated mass/spring system under random forces has been studied. An approximate expression for the local response of the concentrated mass relative to the plate and the inertial displacement of the spring end at its point of connection with the plate has been developed as the asymptotic limit of a classical component modal analysis by using Asymptotic Modal Analysis (AMA). It is shown that when the number of plate modes in the frequency bandwidth is sufficiently large, the AMA result is quite accurate. An exceptional case occurs when the natural frequency of the mass/spring system is inside the bandwidth interval of excitation.

1. INTRODUCTION

At very high frequencies, a dynamic system under band limited random excitation may respond in many modes. It is of interest under these circumstances to investigate the behaviour in the asymptotic limit of many modes responding. Asymptotic Modal Analysis (AMA) [1–10] was developed to provide an alternative to Statistical Energy Analysis (SEA) [11]. AMA provides information on local spatial response and thus is able to distinguish between the response at most spatial points of a dynamical system (which tend to be statistically the same) and certain special points such as a point of external excitation or a point where a discrete or rapid change in the system's dynamical properties may occur, e.g., a concentrated mass attached to a plate. One of the outstanding unresolved questions for both AMA and SEA is how to treat effectively the dynamics of two or more interconnected systems. The failure of SEA to provide consistently accurate results and, heretofore, the absence of any extension of AMA to such systems has been a major limitation for both methods. References [12–15] are representative recent publications that discuss possible approaches based upon SEA ideas or power flow theory. In the present paper, the authors examine a simple prototype of two interconnected dynamical systems, i.e., a uniform elastic plate (or more precisely an elastic plate with smoothly varying mass, stiffness and damping properties) to which is attached a spring/mass/damper system; see Figure 1. This example has interest in its own right and, as will be discussed suggests how more general interconnected systems may be treated within the framework of AMA. The present work is most directly an extension of earlier work by Kubota *et al*. [5]. The reader not already familiar with reference [5] is encouraged to read that paper first as the present paper builds directly from that work. Some readers may find the details of this analysis complex to follow. But each step is clearly explained in reference [5] and the present paper and, given the significance of the results, we believe careful study by the reader will be repaid.

0022–460X/98/250843 + 21 $25.00/0/sv981520

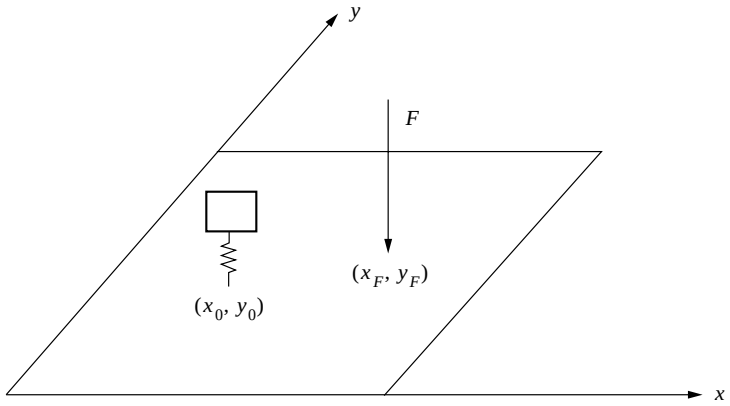

Figure 1. Geometry of the plate structure with concentrated mass/spring system.

2. MODAL ANALYSIS

The elastic plate deflection, w, is expanded in terms of its natural modes, $\psi_m(x, y)$:

$$w(t, x, y) = \sum_m a_m \psi_m(x, y). \tag{1}$$

Note ψ_m are the natural plate modes with no spring/mass/damper attached. The kinetic energy of the plate plus spring/mass/damper system is given by

$$T = \frac{1}{2}\sum_m M_m \dot{a}_m^2 + \frac{1}{2}\sum_m M_0 (\dot{z} + \dot{z}_0)^2$$

and the potential energy by

$$V = \frac{1}{2}\sum_m M_m \omega_m^2 a_m^2 + \frac{1}{2}\sum_m M_0 \omega_0^2 z^2.$$

The Lagrangian is given by

$$L = T - V + \lambda f.$$

Thus, Lagrange's equations of motion are

$$a_m : M_m [\ddot{a}_m + 2\zeta_m \omega_m \dot{a}_m + \omega_m^2 a_m] = F\psi_{mF} + \lambda\psi_{m0} \tag{2}$$

$$z: M_0 [\ddot{z} + \ddot{z}_0] + M_0 \omega_0^2 z = 0; \qquad z_0 : M_0 [\ddot{z} + \ddot{z}_0] = -\lambda, \tag{3a, b}$$

and the equation of constraint is

$$f \equiv \sum_m a_m \psi_{m0} - z_0 = 0. \tag{4}$$

Note z_0 is the inertial displacement of the spring end at its point of connection with the plate, z is the displacement of the mass relative to the plate, and λ is the Lagrange multiplier or force of constraint between the spring and the plate. Also note the damping of the plate

has been included, but not that of the spring/mass/damper system for reasons to be explained in the sequel. Further,

$$M_m \equiv \iint m_p \psi_m^2 \, \mathrm{d}x \, \mathrm{d}y, \qquad \psi_{mF} \equiv \psi_m (x_F, y_F), \qquad \psi_{m0} \equiv \psi_m (x_0, y_0), \tag{5}$$

where the external force acts at x_F, y_F and the spring/mass is attached to the plate at x_0, y_0.

To obtain the transfer functions needed for the interconnected system between the external force F and various responses, simple harmonic motion is assumed. Thus, from equations (2) and (3), we obtain

$$\hat{a}_m = (\hat{F}\psi_{mF} + \hat{\lambda}\psi_{m0})/M_m \, Y_m (\omega), \tag{6}$$

where

$$Y_m (\omega) \equiv -\omega^2 + \omega_m^2 + j2\zeta_m \omega\omega_m, \qquad \hat{z} = \hat{\lambda}/M_0 \, \omega_0^2, \tag{7a}$$

$$\hat{z}_0 = \frac{\hat{\lambda}}{M_0 \, \omega^2} - \hat{z} = \frac{\hat{\lambda}}{M_0}\left[-\frac{1}{\omega_0^2} + \frac{1}{\omega^2}\right], \qquad \hat{z}_0 + \hat{z} = \frac{\hat{\lambda}}{M_0 \, \omega^2}, \tag{7b, c}$$

$$\sum_m \frac{(\hat{F}\psi_{mF} + \hat{\lambda}\psi_{m0})\psi_{m0}}{M_m \, Y_m} - \frac{\hat{\lambda}}{M_0}\left[-\frac{1}{\omega_0^2} + \frac{1}{\omega^2}\right] = 0, \qquad \hat{\lambda} = -\hat{F}H_\lambda, \tag{8}$$

where

$$H_\lambda = \sum_m \frac{\psi_{mF}\psi_{m0}}{M_m \, Y_m} \Bigg/ \left[\sum_m \frac{\psi_{m0}^2}{M_m \, Y_m} + \frac{1}{M_0}\left(\frac{1}{\omega_0^2} - \frac{1}{\omega^2}\right)\right].$$

The following transfer functions are defined and determined.

$$H_z \equiv \frac{\hat{z}}{\hat{F}} = \frac{\hat{z}}{\hat{\lambda}}\frac{\hat{\lambda}}{\hat{F}} = -\frac{1}{M_0 \, \omega_0^2} H_\lambda, \tag{9a}$$

$$H_{z0} \equiv \frac{\hat{z}_0}{\hat{F}} = \frac{\hat{z}_0}{\hat{\lambda}}\frac{\hat{\lambda}}{\hat{F}} = -\frac{1}{M_0}\left(-\frac{1}{\omega_0^2} + \frac{1}{\omega^2}\right) H_\lambda, \tag{9b}$$

$$H_{z+z0} \equiv \frac{\hat{z} + \hat{z}_0}{\hat{F}} = \frac{\hat{z} + \hat{z}_0}{\hat{\lambda}}\frac{\hat{\lambda}}{\hat{F}} = -\frac{1}{M_0 \, \omega^2} H_\lambda. \tag{9c}$$

To find the mean square response of the several displacements of interest, the standard results of random vibration theory are used, e.g.,

$$\Phi_z (\omega) = |H_z (\omega)|^2 \Phi_F (\omega) \tag{10}$$

and

$$\bar{z}^2 = \int \Phi_z \, \mathrm{d}\omega, \tag{11}$$

where Φ_z, Φ_F are the power spectra of response and excitation force, respectively.

Following Kubota *et al*. [5], several results of interest are determined. First consider the natural frequencies (undamped) of the coupled or connected system. The resonant condition is obtained from any one of the transfer functions (for zero damping) as

$$\sum_m \frac{\psi_{m0}^2}{M_m(\omega_m^2 - \omega_M^2)} + \frac{1}{M_0}\left(\frac{1}{\omega_0^2} - \frac{1}{\omega_M^2}\right) = 0. \tag{12}$$

Here the ω_M denote the natural frequencies of the coupled or interconnected system. This result will be useful in what follows. It is not necessary to solve equation (12) *per se* for the purposes of this study. It is sufficient to know that it exists and that in principle the natural frequencies and modes of the interconnected system may be determined.

Now, the solution for the plate (with the spring/mass/damper connected) in terms of the coupled or interconnected natural modes is expanded, i.e.

$$\hat{w}(\omega; x, y) = \sum_M \hat{b}_M(\omega)\phi_M(x, y). \tag{13}$$

Next for $\omega = \omega_M$ and using equations (1) and (13), one obtains

$$\hat{b}_M(\omega_M)\phi_M(x, y) \cong \sum_m \hat{a}_m(\omega_M)\psi_m(x, y). \tag{14}$$

Eliminating ϕ_M from equations (13) and (14) gives

$$\hat{w}(\omega; x, y) \cong \sum_M \frac{\hat{b}_M(\omega)}{\hat{b}_M(\omega_M)} \sum_m \hat{a}_m(\omega_M)\psi_m(x, y). \tag{15}$$

On the other hand, $\hat{b}_M$ may be expressed as

$$\hat{b}_M(\omega) = C_M / Y_M(\omega), \tag{16}$$

where

$$Y_M(\omega) = -\omega^2 + \omega_M^2 + j2\zeta_M \omega_M \omega \qquad \text{and} \qquad C_M = \hat{b}_M(\omega_M) j2\zeta_M \omega_M^2.$$

Thus, equation (15) may be written as

$$\hat{w}(\omega; x, y) \cong \sum_M \frac{2j\zeta_M \omega_M^2}{Y_M(\omega)} \sum_m \hat{a}_m(\omega_M)\psi_m(x, y). \tag{17}$$

Now

$$\hat{z}_0 \equiv \hat{w}(\omega; x_0, y_0) \cong \sum_M \frac{2j\zeta_M \omega_M^2 \hat{z}_0(\omega_M)}{Y_M(\omega)}, \tag{18}$$

$$H_{z0}(\omega) \cong \sum_M \frac{2j\zeta_M \omega_M^2 H_{z0}(\omega_M)}{Y_M(\omega)}. \tag{19}$$

Also, using the usual small damping assumption,

$$\bar{z}_0^2 \cong \sum_{M \varepsilon \Delta\omega} \pi\zeta_M \omega_M |H_{z0}(\omega_M)|^2 \Phi_F(\omega_M), \qquad \bar{z}^2 \cong \sum_{M \varepsilon \Delta\omega} \pi\zeta_M \omega_M |H_z(\omega_M)|^2 \Phi_F(\omega_M), \tag{20a, b}$$

$$\overline{(z + z_0)^2} \cong \sum_{M \varepsilon \Delta\omega} \pi\zeta_M \omega_M |H_{z+z0}(\omega_M)|^2 \Phi_F(\omega_M). \tag{20c}$$

The small damping assumption means that terms of order ζ_M^2 have been consistently neglected compared to unity. Physically it is assumed that the resonant peaks in the transfer function are well separated in frequency. Note also that equation (20a) has neglected products of transfer functions from two different modes, say $M = M_1$ and M_2 for $M_1 \neq M_2$, but included all self products when $M_1 = M_2$, thus reducing a double summation over M to a single summation. Neglecting the cross-transfer functions between two different resonant modes is based upon the notion that the resonant peaks of the transfer function are well separated in frequency for small damping.

Note that equation (20a) and corresponding results for z and $z + z_0$ basically only depend on the observation that equation (16) holds. To determine a useful representation of the several transfer functions, one may proceed as follows.

For $\omega = \omega_M$, the denominator of equation (8) becomes, using equation (12),

$$\sum_m \frac{\psi_{m0}^2}{M_m\, Y_m\,(\omega_M)} + \frac{1}{M_0}\left(\frac{1}{\omega_0^2} - \frac{1}{\omega_M^2}\right) \cong -2j \sum_m \frac{\zeta_m\, \omega_m\, \omega_M\, \psi_{m0}^2}{M_m\,(\omega_m^2 - \omega_M^2)^2}. \tag{21}$$

Also, for $\omega = \tilde{\omega}_M \cong \omega_M\,(1 + j\zeta_M)$, the denominator of equation (8) is zero, i.e.,

$$\sum_m \frac{\psi_{m0}^2}{M_m\, Y_m\,(\tilde{\omega}_M)} - \frac{1}{M_0\,\tilde{\omega}_M^2} + \frac{1}{M_0\,\omega_0^2} = 0. \tag{22}$$

For small damping, equation (22) becomes

$$\sum_M \frac{\zeta_m\, \omega_m\, \omega_M\, \psi_{m0}^2}{M_m\,(\omega_m^2 - \omega_M^2)^2} \cong \zeta_M\, \omega_M^2 \left[\sum_m \frac{\psi_{m0}^2}{M_m\,(\omega_m^2 - \omega_M^2)^2} + \frac{1}{M_0\,\omega_M^4}\right]. \tag{23}$$

As an aside, note that equation (23) may be solved for ζ_M once ω_M is known from equation (22). Thus, if $\zeta_m\, \omega_m = \zeta_c\, \omega_c$ for all m, one may conclude that $\zeta_M\, \omega_M \cong \zeta_c\, \omega_c$.

Using equations (9c), (21) and (23) and again recalling the results of reference [5],

$$|H_{z+z0}\,(\omega_M)|^2 \cong \frac{s_1}{4M_0^2\zeta_M^2\omega_M^8[s_2 + M_p\,/M_0\,\omega_M^4]^2}, \tag{24}$$

where

$$s_1 \equiv \sum_m \sum_n \frac{\psi_{mF}\,\psi_{m0}\,\psi_{nF}\,\psi_{n0}}{\langle\psi_m^2\rangle\langle\psi_n^2\rangle[\omega_m^2 - \omega_M^2]\,[\omega_n^2 - \omega_M^2]}, \tag{25}$$

$$s_2 \equiv \sum_m \frac{\psi_{m0}^2}{\langle\psi_m^2\rangle[\omega_m^2 - \omega_M^2]^2} \tag{26}$$

and $\langle \cdots \rangle$ denotes the spatial average.

Note equations (24–26) have used the small damping approximation. Now using equations (20a) and (24),

$$\overline{(z_0 + z)^2} \cong \frac{\pi}{4} \sum_{M \epsilon \Delta\omega} \frac{\Phi_F\,(\omega_M)}{M_p^2 \omega_M^3 \zeta_M}\, g(\omega_M), \tag{27a}$$

where

$$g(\omega_M) = \left(\frac{M_p}{M_0\,\omega_M^2}\right)^2 \frac{s_1}{[s_2 + M_p/M_0\,\omega_M^4]^2}. \tag{28a}$$

The expression for $g(\omega_M)$ may be rewritten [5] using

$$\omega_M^4 s_1 \cong \omega_M^4 s_2 \cong \frac{\pi^2 M^2}{4} + \left(\frac{M_p}{M_0}\right)^2,$$

where M is the modal number.

Now as shown by Kubota *et al*. [5], the wavelength of a high frequency plate mode, λ_p, may be expressed as

$$\lambda_p^2 M = \pi A_p,$$

where A_p is the plate area.

Thus,

$$M = \frac{\pi A_p}{\lambda_p^2}$$

and

$$\omega_M^4 s_1 = \frac{\pi^4}{4}\frac{A_p^2}{\lambda_p^4} + \left(\frac{M_p}{M_0}\right)^2.$$

Finally then,

$$g(\omega_M) = \frac{(2m_p\,\lambda_p^2/M_0\,\pi^2)^2}{[1 + (2m_p\,\lambda_p^2/M_0\,\pi^2)^2]}\frac{1}{[1+\mu_m]^2}, \tag{28b}$$

where $\mu_m = (M_p/M_0)/[(\pi^4/4A_p^2/4\lambda_p^4) + (M_p/M_0)^2]$, and this term is usually small compared to unity and can be neglected.

Note equation (27a) is the same result obtained in reference [5] for a *rigidly* connected mass, i.e., $\omega_0 \to \infty$ and $z \to 0$, $z_0 + z \to z_0$.

For ω_0 finite and $z \neq 0$,

$$|H_z(\omega_M)|^2 = \frac{\omega_M^4}{\omega_0^4}|H_{z+z0}|^2, \qquad |H_{z0}(\omega_M)|^2 = \left(1 - \frac{\omega_M^2}{\omega_0^2}\right)^2 |H_{z+z0}|^2. \tag{29a, 30a}$$

Analogously, following equation (27a),

$$\bar{z}^2 = \frac{\pi}{4}\sum_{M\varepsilon\Delta\omega}\frac{\omega_M^4}{\omega_0^4}\frac{\Phi_F(\omega_M)g(\omega_M)}{M_p^2\omega_M^3\zeta_M}, \tag{29b}$$

$$\bar{z}_0^2 = \frac{\pi}{4}\sum_{M\varepsilon\Delta\omega}\left(1 - \frac{\omega_M^2}{\omega_0^2}\right)^2\frac{\Phi_F(\omega_M)g(\omega_M)}{M_p^2\omega_M^3\zeta_M}. \tag{30b}$$

Note that when equation (28a) is used this is called the exact result. Equation (28b) corresponds to the approximately exact result.

3. THE ASYMPTOTIC LIMIT

Now if the frequency bandwidth of excitation is sufficiently small, then ω_M, ζ_M, $\Phi_F(\omega_M)$ will be slowly varying and may be approximated by their centre frequency counterparts, ω_c, ζ_c, $\Phi_F(\omega_c)$. Thus, equations (27), (29b) and (30b) become

$$\overline{(z_0 + z)^2} \cong \frac{\pi}{4} \frac{\Phi_F(\omega_c)}{M_p^2 \omega_c^3 \zeta_c} \sum_M g(\omega_M). \tag{27b}$$

But

$$\sum_M g(\omega_M) \cong \Delta M g(\omega_c),$$

where ΔM is the number of modes in the frequency interval, $\Delta\omega$, and thus

$$\overline{(z_0 + z)^2} \cong \frac{\pi}{4} \frac{\bar{F}^2_{\Delta\omega}}{M_p^2 \omega_c^3 \zeta_c} \frac{\Delta M}{\Delta\omega} g(\omega_c), \tag{27c}$$

where $\bar{F}^2_{\Delta\omega} \equiv \Phi_F(\omega_c)\Delta\omega$ is the mean square force of excitation. Further the factor multiplying $g(\omega_c)$ on the right side of equation (27b) can be identified with the mean square response of the plate at all points except near the point of excitation (where the response is higher [2]) and, of course, at the point where the spring/mass/damper is attached to the plate.

Similarly, equations (29b) and (30b) may be approximated asymptotically as

$$\bar{z}^2 \cong \frac{\pi}{4} \frac{\bar{F}^2_{\Delta\omega}}{M_p^2 \omega_c^3 \zeta_c} \frac{\Delta M}{\Delta\omega} g(\omega_c) \frac{\omega_c^4}{\omega_0^4} \tag{29c}$$

$$\bar{z}_0^2 \cong \frac{\pi}{4} \frac{\bar{F}^2_{\Delta\omega}}{M_p^2 \omega_c^3 \zeta_c} \frac{\Delta M}{\Delta\omega} g(\omega_c) \left(1 - \frac{\omega_c^2}{\omega_0^2}\right)^2. \tag{30c}$$

Note in equation (30c) the factor $(1 - \omega_c^2/\omega_0^2)^2$ must be a reasonable approximation to the factor $(1 - \omega_M^2/\omega_0^2)^2$ throughout the bandwidth of excitation. For this to be true ω_0 must be sufficiently outside the bandwidth interval of excitation, $\Delta\omega$. Hence, the damping term previously omitted plays no essential role if the spring/mass/damper is lightly damped. Conversely if the spring/mass/damper system were heavily damped, then the factor described above could be replaced by a slowly varying (with frequency) term dominated by the damping. Indeed as with many "good approximations", one finds that even when ω_0 is in the frequency bandwidth interval of excitation, these equations may be reasonably accurate except in the statistically exceptional case when ω_0 is very near one of the ω_M. See the subsequent discussion in section 4.

Equations (27c), (29c), and (30c) are the mean square response of the discrete mass in an inertial co-ordinate system, the corresponding response of the mass relative to the plate and the inertial response of the plate at the point of the spring/mass/damper system attachment to the plate, respectively.

It may be of interest to note that the energy method used in this paper (variational principle plus constraint equations using Lagrange multipliers) is completely equivalent to the mobility method. So if one used the mobility formalism *and* the AMA methodology, one would obtain the same results.

4. NUMERICAL EXAMPLES

In order to illustrate the accuracy of the results, a few numerical examples for a rectangular plate have been considered as shown in Figure 1. The results from the asymptotic method, i.e., equations (29c) and (30c), are compared to both exact solutions using equations (27a) and (28a) and approximately exact solutions using equations (29b), (30b) and (28b).

4.1. EXAMINATION OF AN APPROXIMATE ASSUMPTION

In the asymptotic modal analysis, for high order modes, a useful approximation is

$$\Delta M \simeq \Delta\Omega, \tag{31}$$

where ΔM is the number of modes in the non-dimensional frequency interval, $\Delta\Omega$ and $\Delta\Omega = \Omega_{max} - \Omega_{min}$. The non-dimensional frequency Ω can be defined as

$$\Omega \equiv \omega(A_p/4\pi)\sqrt{m_p/D}.$$

For simplicity, a uniform, all simply supported aluminum plate of length l_x and width l_y is considered. The dimensions of the plate are $1200 \times 800 \times 2$(mm). The attachment point (x_0, y_0) (or local response point) for the mass/spring system and the excitation point (x_F, y_F) are located at $x_0/l_x = y_0/l_y = 1/\pi$ and $x_F/l_x = 2/\pi$, $y_F/l_y = 1/2\pi$, respectively. The attachment mass weight is 110 g and the spring stiffness at the attachment point can be adjusted to illustrate different conditions. The eigenmode function and the non-dimensionalized mode frequency are

$$\psi_m(x, y) = \sin(m_x \pi x/l_x) \sin(m_y \pi y/l_y) \tag{32}$$

$$\Omega_m = (\pi/4\alpha)[(\alpha m_x)^2 + m_y^2], \tag{33}$$

where m_x, m_y are the integers defining the mth plate mode and α is the plate aspect ratio; $\alpha \equiv l_y/l_x$.

Figure 2 shows the number of modes, ΔM, in $\Delta\Omega$ versus the centre frequency of a one-third octave band for different numbers of total modes, M. In this figure, the solid line indicates the number of modes, ΔM, as determined by equation (31). For a one-third octave band, $\Omega_{max} = 2^{1/6}\Omega_c$, $\Omega_{min} = (1/2)^{1/6}\Omega_c$ and Ω_c is the non-dimensional centre frequency.

For simplicity, it is often convenient to include the same modal number in both the x- and y-directions. However, this does not automatically insure that all modes in a given frequency band are included. To illustrate this, consider the following.

The symbol, $\diamond$, with broken line indicates the theoretical results for $M = 225$, i.e., $m_{x,max} = 15$, $m_{y,max} = 15$ and a non-dimensional natural frequency of the spring/mass system of $\Omega_0 = 150$. The modal frequency, ω_M, of the plate with a spring/mass attached is calculated using equation (12). For a given centre frequency, and corresponding one-third octave band, ΔM can be obtained from the set of modal frequencies, ω_M. For $M = 225$, the maximum modal frequency is $\omega_{M,max} = 2417$ (Hz). The error in using equation (31) increases beyond $\omega_c = 1000$ (Hz). The symbol, $\square$, with a broken line indicates the theoretical results for $M = 676$, i.e., $m_{x,max} = 26$, $m_{y,max} = 26$. The maximum modal frequency is $\omega_{M,max} = 7278$ (Hz). The error in using equation (31) increases beyond $\omega_c = 2531$ (Hz). The symbol, $\triangle$, with a dot-dash line indicates the theoretical results for $M = 1225$ i.e., $m_{x,max} = 35$, $m_{y,max} = 35$. The maximum modal frequency is $\omega_{M,max} = 13\,189$ (Hz). The error in using equation (31) is now small until the centre frequency reaches 6400 (Hz). From this figure, it may be concluded that the maximum number of modes required for good accuracy depends upon the maximum modal frequency which must be greater than about twice the maximum excitation centre frequency. A more efficient counting of

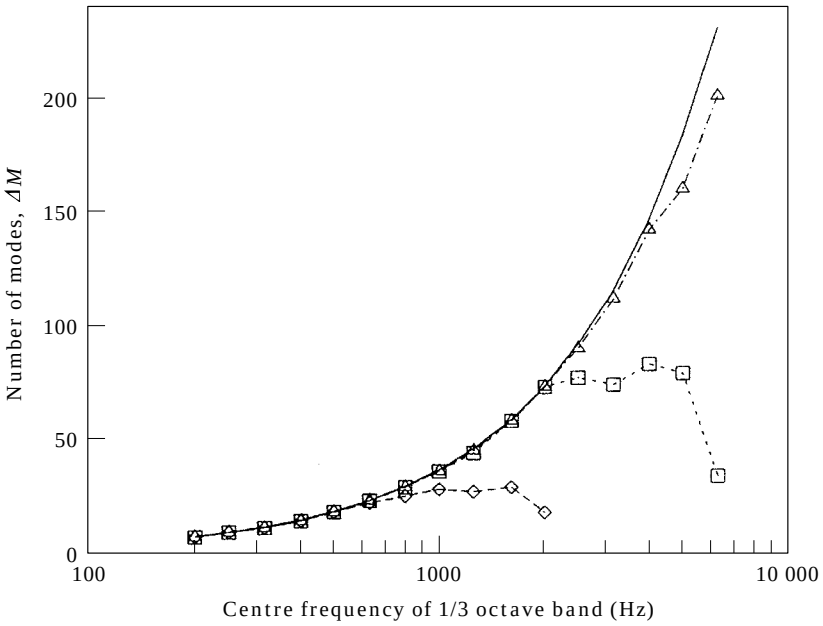

Figure 2. The number of modes, ΔM, in $\Delta\Omega$ versus the centre frequency of a one-third octave band for different total modes M: ——, $\Delta\Omega$; —◇—, $M=225$; —□—, $M=676$; —△—, $M=1225$.

modes would use an algorithm that insures only modes in a given frequency interval are included [5]. However, this is more tedious to program.

Note that consistent with equation (31) is the observation that the modes are equally spaced in the frequency interval.

4.2. COMPARISON WITH EXACT RESULTS FOR A RANDOM FORCE ACTING ON THE PLATE

In this case, a point random force, F, is acting at the point, (x_F, y_F), of the plate. In order to illustrate the accuracy of equations (29c) and (30c), a comparison with the exact results of equations (29b) and (30b) using equation (28) has been made. The ratios of asymptotic to exact results, Rz, Rzo and $Rzzo$, are defined as

$$Rz \equiv \frac{\text{equation (29c)}}{\text{equation (29b)}}, \qquad Rzo \equiv \frac{\text{equation (30c)}}{\text{equation (30b)}}, \qquad Rzoz \equiv Rzo/Rz.$$

Figure 3(a) and (b) show Rz and Rzo versus the centre frequency of a one-third octave band for an attachment mass weight $M_0 = 110$ g, total modal number, $M = 1225$, and three different non-dimensional natural frequencies of the spring/mass system. In these figures, the symbols, □, with broken line, ◇, with solid line and △, with dot-dash line indicate the theoretical results for $\Omega_0 = 30$, 150 and 1000, respectively. From Figure 3(a), it is seen that Rz is virtually independent of Ω_0. The values of Rz and Rzo oscillate about unity. From Figure 3(b), it is found that a larger error in Rzo occurs in the frequency region where the excitation centre frequency is close to the natural frequency of the spring/mass system. For $\Omega_0 = 150$ (949 Hz), Rzo reaches 0·54 at the centre frequency, $\omega_c = 1000$ (Hz). For $\Omega_0 = 1000$ (6329 Hz), Rzo reaches 1/40·88 at the centre frequency, $\omega_c = 6400$ (Hz). However, fortunately, the errors are of little practical consequence as will be seen in the sequel.

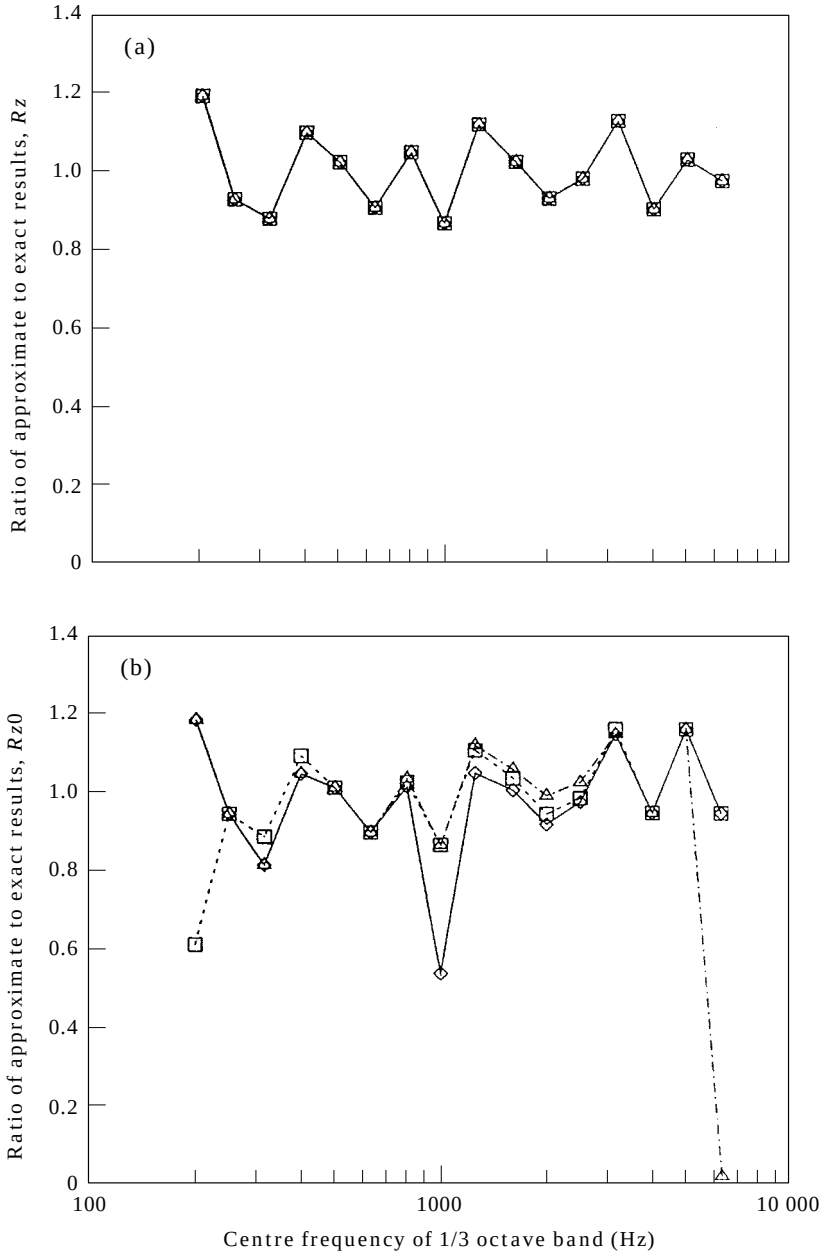

Figure 3. The ratio of approximate to exact results for (a) Rz and (b) $Rz0$ versus the centre frequency of a one-third octave band for total modal number $M = 1225$: —□—, $\Omega_0 = 30$; —◇—, $\Omega_0 = 150$; —△—, $\Omega_0 = 1000$.

Similar results are also shown in Figure 4 for the relative mean-square response, $Rzzo$. The figure construction is the same as those in Figure 3. The values of $Rzzo$ for all three cases are approximately unity except near the resonant frequencies.

Figure 5(a) and (b) show Rz and Rzo versus the centre frequency of a one-third octave band for an attachment mass weight, $M_0 = 110$ g, $\Omega_0 = 150$ and two different total modal numbers, M. The symbols, ◇, with solid line, and △, with dot-dash line indicate the theoretical results for $M = 1225$ and 676, respectively. Note in the higher frequency range

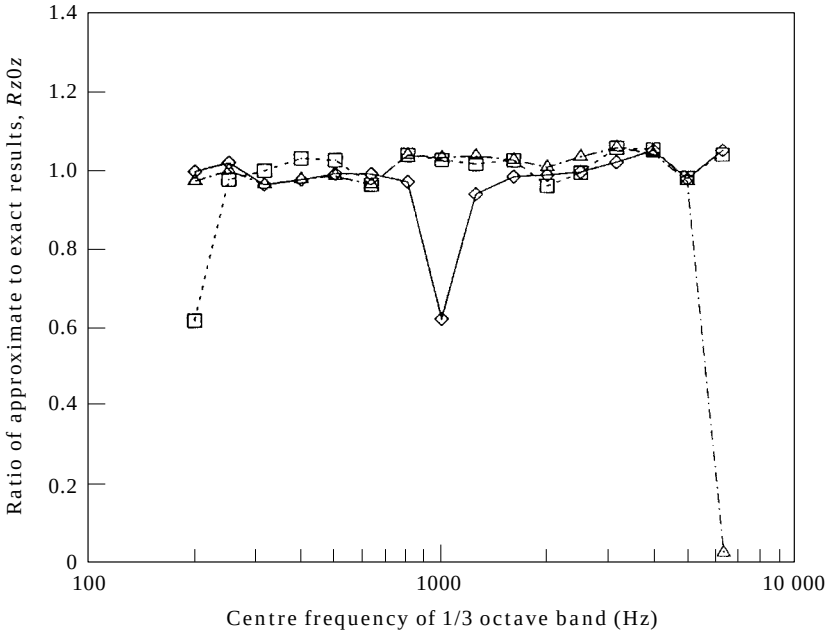

Figure 4. The ratio of approximate to exact results of $Rzz0$ versus the centre frequency of a one-third octave band for total modal number $M = 1225$: —□—, $\Omega_0 = 30$; —◇—, $\Omega_0 = 150$; —△—, $\Omega_0 = 1000$.

the results for large M are (slightly) better. However, the significant observation is that the results are overall relatively insensitive to M, if M is sufficiently large.

From these figures, it may be concluded that the present asymptotic method has good accuracy except for excitation near the resonant spring–mass frequencies.

4.3. COMPARISON WITH EXACT RESULTS FOR A RANDOM FORCE ACTING DIRECTLY ON THE MASS/SPRING SYSTEM

When a random force is applied to the mass/spring system rather than to the plate, Lagrange's equations of motion become

$$a_m : M_m [\ddot{a}_m + 2\zeta_m \omega_m \dot{a}_m + \omega_m^2 a_m] = \lambda \psi_{m0}, \tag{34}$$

$$z: M_0 [\ddot{z} + \ddot{z}_0] + M_0 \omega_0^2 z = F, \tag{35a}$$

$$z_0 : M_0 [\ddot{z} + \ddot{z}_0] = F - \lambda. \tag{35b}$$

After an analogous derivation to that performed previously in sections 2 and 3, the same exact expression for $\overline{z_0 + z}^2$ is obtained, as shown in equations (27a) and (28a), but now $s_1 \equiv M_p^2/M_0^2\omega_M^4$ rather than as given by equation (25) and the corresponding expression for $g(\omega_M)$ is also changed. For further details, see Appendix A.

The approximate exact expressions for $\bar{z}^2$ and $\bar{z}_0^2$ are also the same as shown in equations (29b) and (30b), but now

$$g(\omega_M) = \frac{(2m_p \lambda_p^2/M_0 \pi^2)^4}{[1 + (2m_p \lambda_p^2/M_0 \pi^2)^2]^2} \frac{1}{[1 + \mu_m]^2}. \tag{28c}$$

As compared with equation (28b), it is found that equation (28c) is the square of equation (28b) when μ_m is neglected compared to unity.

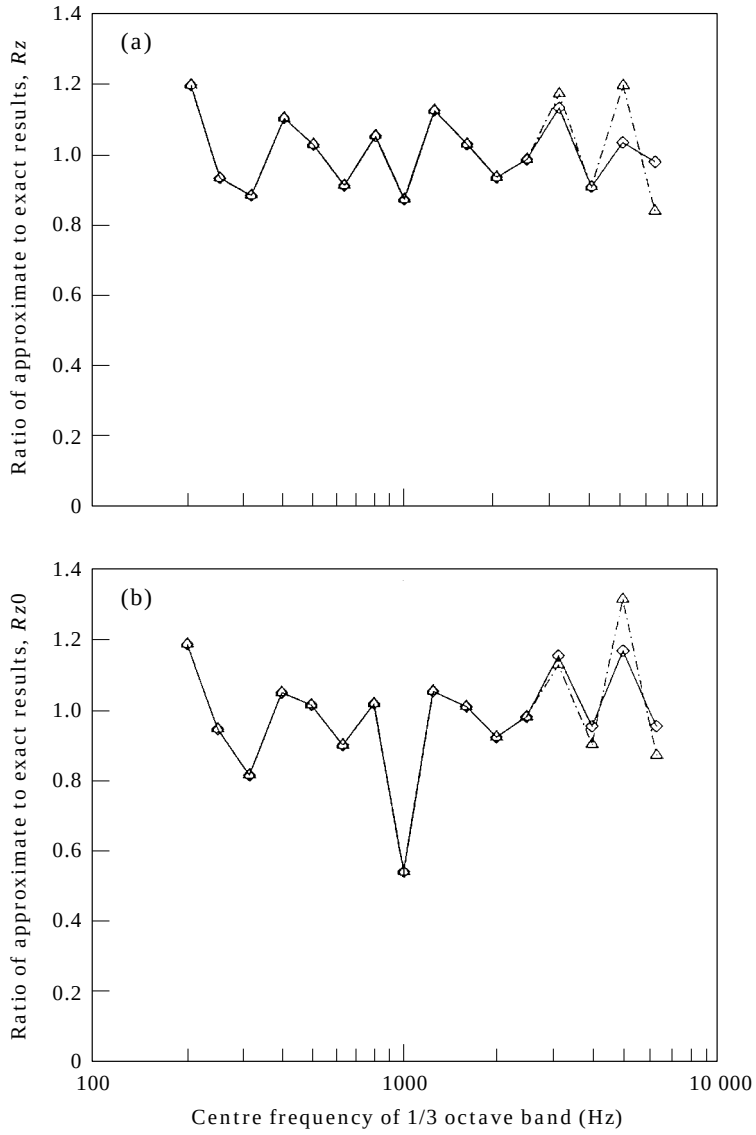

Figure 5. The ratio of approximate to exact results for (a) Rz and (b) $Rz0$ versus the centre frequency of a one-third octave band for $\Omega_0 = 150$ and different total modal number: —◇—, $M = 1225$; —△—, $M = 676$.

As a numerical example, the same model as described in section 4.2 is used. For comparison with the results obtained from section 4.2, Rp_z, Rp_{z0} and Rp_{z+z0} are used to indicate the ratios of the present mean-square resonses $\bar{z}^2$, $\bar{z}_0^2$ and $(\overline{z+z_0})^2$ to those obtained in section 4.2 for the case where the plate is directly excited. The ratios of Rp_z, Rp_{z0} and Rp_{z+z0} are defined as

$$Rp_z \equiv \frac{\text{equation } (A16)\,[\text{using equation } (A21)]}{\text{equation (29b)}\,[\text{using equation (28a)}]},$$

$$Rp_{z0} \equiv \frac{\text{equation } (A19)\,[\text{using equation } (A21)]}{\text{equation (30b)}\,[\text{using equation (28a)}]},$$

$$Rp_{z+z0} \equiv \frac{\text{equation (A20) [using equation (A21)]}}{\text{equation (27a) [using equation (28a)]}}.$$

The results are shown in Figure 6. The symbols, $\square(\Omega_0 = 30)$, $\diamond(\Omega_0 = 150)$, and $\triangle(\Omega_0 = 1000)$, with broken and solid lines indicate the results for $\bar{z}^2$ and $\bar{z}_0^2$, respectively. Both Rp_z and Rp_{z0} are almost unity except for the smaller excitation frequency as shown in Figure 6(a). As the excitation frequency increases, the ratios Rp_z and Rp_{z0} are virtually independent of the natural frequency of mass/spring system.

Figure 6(b) shows the results for the mean-square responses $(\overline{z+z0})^2$. The $z+z0$ response for the random force acting directly on the mass/spring system is smaller than that for the random force acting on the plate, and as the excitation frequency increases,

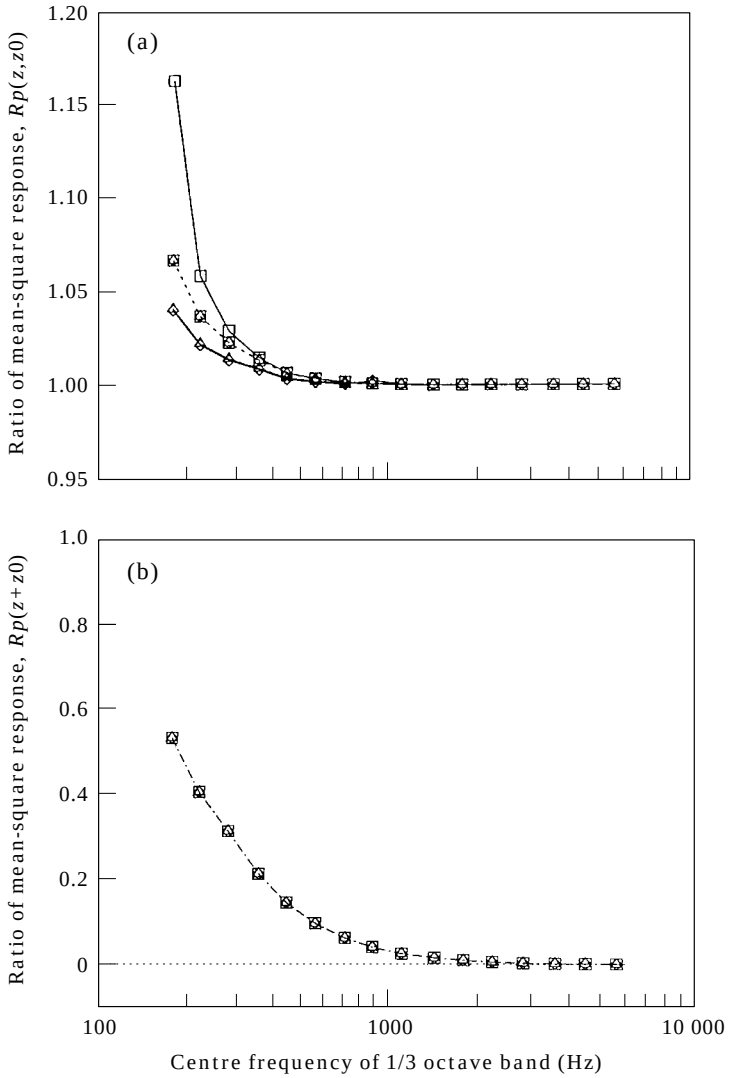

Figure 6. The ratio of mean-square response for the random force acting directly on the mass/spring system to those for the random force acting on the plate. The symbols, $\square(\Omega_0 = 30)$, $\diamond(\Omega_0 = 150)$ and $\triangle(\Omega_0 = 1000)$ with broken, solid lines and dot-dash line indicate the results for (a) $\bar{z}^2$, $\overline{z0}^2$ and (b) $(\overline{z+z0})^2$, respectively.

the ratio Rp_{z+z0} decreases and approaches zero. The ratio Rp_{z+z0} is also virtually independent of the natural frequency of the mass/spring system.

4.4. ACCELERATION RESPONSE AND COMPARISON WITH EXPERIMENTAL AND APPROXIMATELY EXACT RESULTS

A slightly different numerical model is examined now corresponding to the experimental model studied in reference [5]. An aluminum plate was suspended by four rubber bands in a non-rectangular reverberation room of volume 245 m^3. The boundary conditions for the plate are thus for freely supported edges. Of course, the AMA theory predicts that in the limit of many modes in a bandwidth, the results are independent of the boundary conditions. The plate was excited using a loudspeaker driven by white noise. In this numerical example, the attachment point for the mass/spring system is located at $l_x = 800$ (mm), $l_y = 300$ (mm) with a mass weight of 110 g. The natural frequency of this spring/mass system is varied in our numerical examples. In the experiment, ω_0, $\Omega_0 \to \infty$, i.e., the mass was rigidly attached to the plate. The measured plate response was taken as an average value over three measurement points ($l_x = 150$, 550, 750 (mm), $l_y = 150$, 350, 550 (mm)), respectively. For the purpose of this paper it is not necessary to consider the damping and the radiation efficiency of the plate *per se* or the sound excitation level, and the theoretical result for the plate response without the concentrated mass is used to normalize the present results.

Figures 7(a)–(c) show the acceleration level at the attachment point of the spring/mass for three different spring/mass natural frequencies, $\Omega_0 = 30$, 150 and 1000. The broken and dot-dash lines indicate the acceleration responses, z_0 and z, respectively. The results are from the asymptotic method, i.e., equations (29c) and (30c). The theoretical and experimental results for a plate carrying a concentrated mass that is rigidly connected (no spring) (ω_0 or $\Omega_0 \to \infty$) are also plotted in these figures. They are indicated by the solid line (theory) and symbol $\square$ (experiment) for the mass response without spring and the broken line and symbol $\triangle$ for the plate response without spring, respectively.

For $\Omega_0 = 30$ (190 Hz) (which is lower than the minimum excitation centre frequency, $\Omega_c = 31{\cdot}6$ (200 Hz)), the mass response with a spring is larger than the concentrated mass response without a spring, and z_0 and z have nearly the same response level in the higher frequency range as shown in Figure 7(a).

For $\Omega_0 = 1000$ (6329 Hz) (which is near the maximum excitation centre frequency, $\Omega_c = 1011$ (6400 Hz)), the z_0 response almost coincides with the concentrated mass response ($\Omega_0 \to \infty$) except near the resonant frequency at 6400 Hz, where the z response is very small, as shown in Figure 7(c). Note that if $\Omega_0 \to \infty$ then $z \to 0$ and $z_0 \to$ the concentrated mass response with the mass rigidly attached to the plate.

When Ω_0 is in the middle of the frequency range, e.g., $\Omega_0 = 150$ (949 Hz), the minimum response for z_0 occurs near the resonant spring/mass frequency and the corresponding z response is close to the concentrated mass response without the spring. In the lower frequency range ($\Omega < \Omega_0$), the z_0 response coincides with the concentrated mass response without the spring and the z response becomes very small. In the higher frequency range ($\Omega > \Omega_0$), both z_0 and z response levels are between the concentrated mass and plate response levels without the spring, and approach the plate response level as the frequency increases, as shown in Figure 7(b). Note that spring–mass acts as a local vibration absorber for the plate and the plate response is indeed less than the spring–mass for excitation frequencies near Ω_0.

Figure 8 shows a comparison of acceleration levels as obtained from the asymptotic limit using equations (29c) and (30c) and from the approximately exact results using equations (29b), (30b) and (28b) for $\Omega = 150$ and $M = 1225$ modes. The asymptotic results for z and

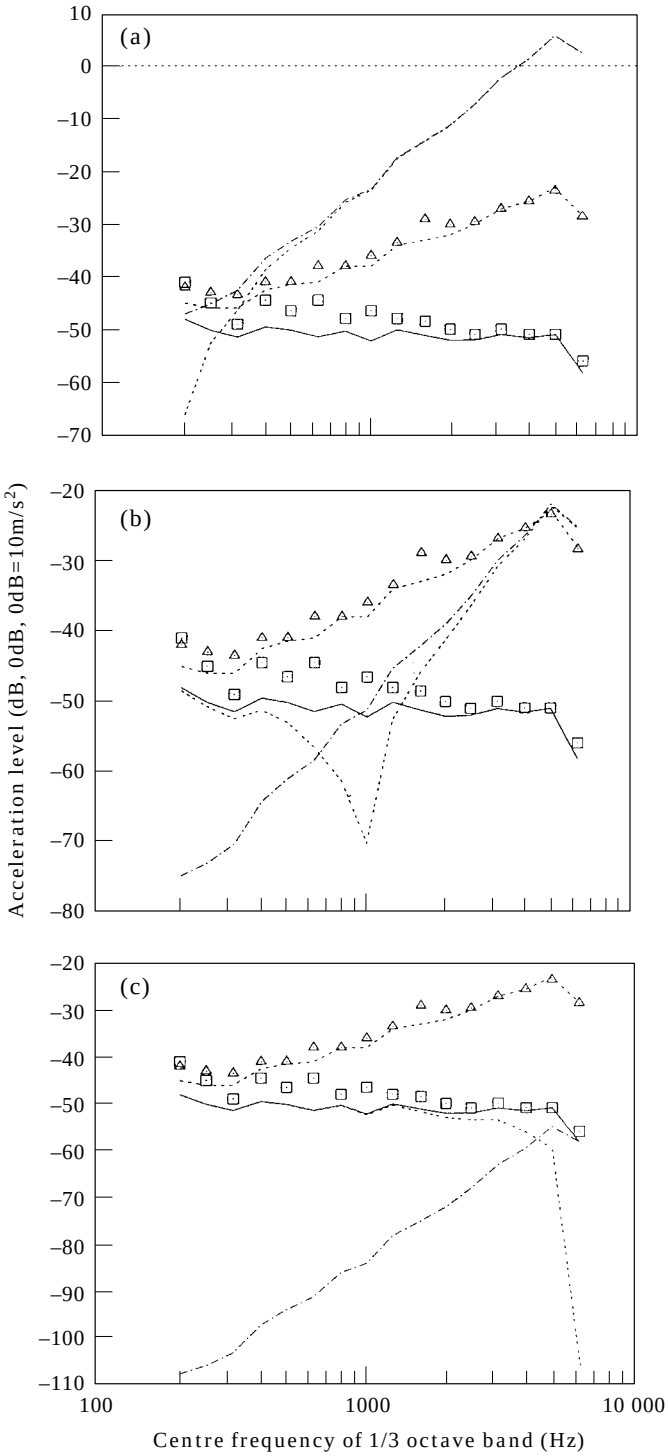

Figure 7. The acceleration response level versus the centre frequency of a one-third octave band for (a) $\Omega_0 = 30$, (b) $\Omega_0 = 150$, (c) $\Omega_0 = 1000$. —— and □, theoretical and experimental concentrated mass response without spring; –– and △, theoretical and experimental averaged plate response over three points without spring; ——––, z_0 response with spring; – · –, z response with spring.

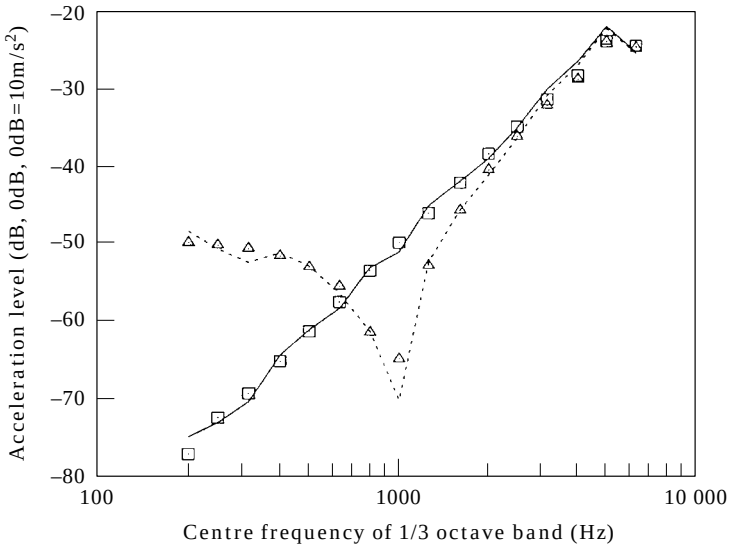

Figure 8. Comparison of acceleration response level between the approximately exact and asymptotic results: △ and □, approximately exact result for z_0 and z; –– and ——, asymptotic results z_0 and z.

z_0 are indicated by the solid and broken lines, respectively. The approximately exact results for z and z_0 are indicated by the symbols □ and △, respectively. The agreement between these two results is excellent except near the resonant spring/mass frequency.

Now it is clear that the "errors" discussed previously (recall Figures 3 and 4) occur when the plate response, z_0, is at a minimum and the mass response relative to the plate, z, dominates. So an error in z_0 is of little practical consequence and z is predicted accurately by the asymptotic approach.

5. POSSIBLE GENERALIZATIONS TO MORE COMPLEX INTERCONNECTED SYSTEMS

There are several possible directions for generalizing the present results. Some are immediate. Others require additional work. Consider the array of configurations shown in Figures 9. Figure 9(a) shows two spring/mass/dampers attached to the plate. The present results apply independently to each spring/mass/damper system (provided the two systems are separated by at least one wavelength of the plate response in the frequency range of interest). In Figure 9(b), a higher dimensional spring/mass/damper system is shown. If the natural frequencies of each mode of the higher dimensional system are discrete, well separated and satisfy the conditions of the present asymptotic analysis, then each mode of the spring/mass/damper system may be treated separately as in the present analysis. Under the same circumstances, the generalization to a continuous elastic system is immediate; see Figure 9(c).

Although it requires some additional investigation, generalizations of the present analysis to configurations such as those shown in Figure 9(d), a plate with a stiffener, and Figure 9(e), a frame structure, appear possible.

An interesting open question is what happens when both components of the interconnected system are in the asymptotic limit of many modes responding.

Also, as has been noted previously it has been assumed that the damping in the system is small, i.e., much less than its critical value. It would be interesting to examine larger values of damping, of course. Also the damping of the spring–mass system has been

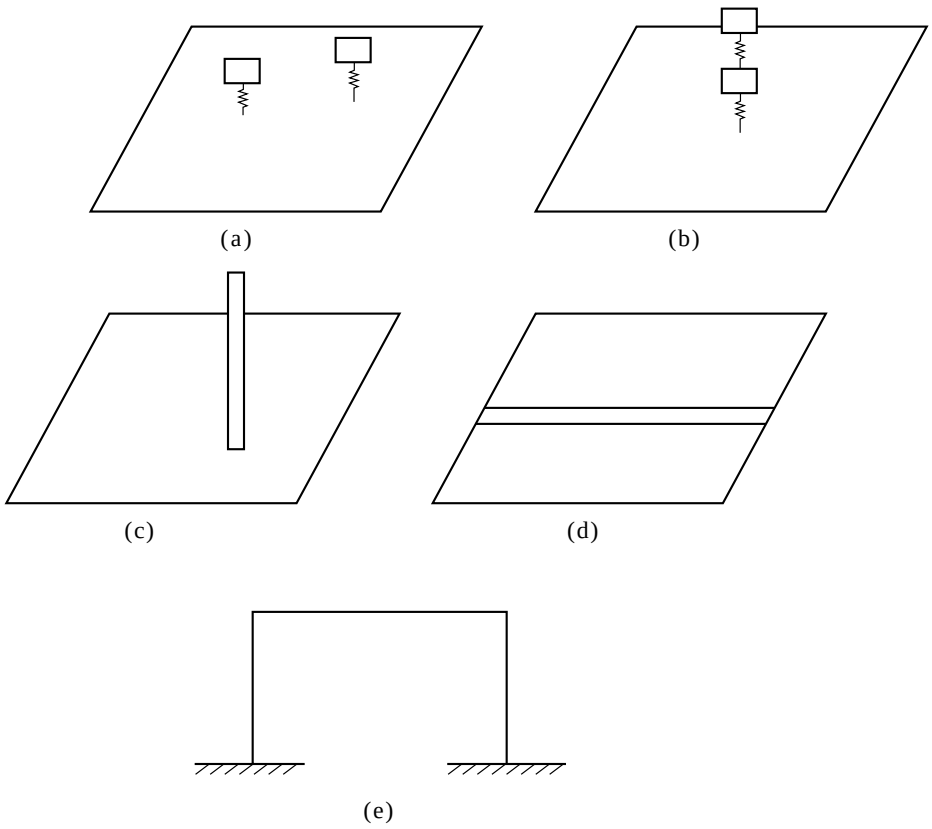

Figure 9. Possible generalizations ((a)–(e)) to more complex interconnected systems.

neglected altogether. This is largely for convenience. Even for small damping, there are three cases, i.e., the damping of the spring–mass is small, comparable or large relative to that of the plate. In the present paper, the first case was primarily considered.

6. CONCLUSIONS

An asymptotic modal analysis has been developed for a prototypical interconnected system. This provides a paradigm for the analysis of an interesting class of such systems.

ACKNOWLEDGMENTS

This work was supported, in part, under AFOSR Grant, ''Limit Cycle Oscillations and Nonlinear Aeroelastic Wing Response''. Major Brian Sanders and Dr C. I. ''Jim'' Chang are the grant monitors.

REFERENCES

1. Y. KUBOTA and E. H. DOWELL 1985 *Journal of Applied Mechanics* **52**, 949–957. Asymptotic modal analysis and statistical energy analysis of dynamical systems.
2. Y. KUBOTA and E. H. DOWELL 1986 *Journal of Sound and Vibration* **106**, 203–216. Experimental investigation of asymptotic modal analysis for a rectangular plate.

3. Y. KUBOTA and E. H. DOWELL 1987 *Journal of the Acoustical Society of America* **81**, 1267–1272. Asymptotic modal analysis for dynamic stresses of a plate.
4. Y. KUBOTA, H. D. DIONNE and E. H. DOWELL 1988 *Journal of Vibration, Acoustics, Stress, and Reliability in Design* **110**, 371–376. Asymptotic modal analysis and statistical energy analysis of an acoustic cavity.
5. Y. KUBOTA, S. SEKIMOTO and E. H. DOWELL 1990 *Journal of Sound and Vibration* **138**, 321–330. The high-frequency response of a plate carrying a concentrated mass.
6. L. PERETTI and E. H. DOWELL 1992 *ASME Journal of Vibration and Acoustics* **114**, 546–554. Experimental verification of the asymptotic modal analysis method as applied to a rectangular acoustic cavity excited by structural vibration.
7. L. PERETTI and E. H. DOWELL 1992 *AIAA Journal* **30**, 1199–1206. A study of intensification zones in a rectangular acoustic cavity.
8. L. PERETTI and E. H. DOWELL 1992 *AIAA Journal* **30**, 1191–1198. Asymptotic modal analysis of a rectangular acoustic cavity excited by wall vibration.
9. Y. KUBOTA and E. H. DOWELL 1992 *Journal of the Acoustical Society of America* **92**, 1106–1112. Asymptotic modal analysis for sound fields of a reverberant chamber.
10. S. DOHERTY and E. H. DOWELL 1994 *Journal of Sound and Vibration* **170**, 671–681. Experimental study of asymptotic modal analysis applied to a rectangular plate with concentrated masses.
11. R. H. LYON 1975 *Statistical Energy Analysis of Dynamical Systems*: *Theory and Application*. Cambridge, MA: MIT Press.
12. S. FINNVEDEN 1995 *Journal of Sound and Vibration* **187**, 495–530. Ensemble averaged vibration energy flows in a three-element structure.
13. A. CARCATERRA and A. SESTIERI 1995 *Journal of Sound and Vibration* **188**, 269–282. Energy density equations and power flow in structures.
14. A. SESTIERI and A. CARCATERRA 1995 *Journal of Sound and Vibration* **188**, 283–296. An envelope energy model for high frequency dynamic structures.
15. E. REBILLARD and J. L. GUYADER 1995 *Journal of Sound and Vibration* **188**, 435–454. Vibration behavior of a population of coupled plates: hyper-sensitivity to the connexion angle.

APPENDIX A: DERIVATION OF $g(\omega_M)$

To obtain the transfer functions needed for the interconnected system between the external force F and various responses, simple harmonic motion is assumed. Thus, from equations (34) and (35), one obtains

$$\hat{a}_m = \hat{\lambda}\psi_{m0}/M_m\, Y_m(\omega), \tag{A1}$$

where

$$Y_m(\omega) \equiv -\omega^2 + \omega_m^2 + j2\zeta_m\,\omega\omega_m \tag{A2}$$

$$\hat{z} = \hat{\lambda}/M_0\,\omega_0^2, \qquad \hat{z}_0 = \frac{\hat{\lambda}}{M_0}\left(\frac{1}{\omega^2} - \frac{1}{\omega_0^2}\right) - \frac{\hat{F}}{M_0\,\omega^2}. \tag{A3}$$

From the equation of constraint of equation (4), one obtains

$$\hat{\lambda}\left[\sum_m \frac{\psi_{m0}^2}{M_m\, Y_m} - \frac{1}{M_0}\left(\frac{1}{\omega^2} - \frac{1}{\omega_0^2}\right)\right] + \frac{\hat{F}}{M_0\,\omega^2} = 0. \tag{A4}$$

The following transfer functions are defined and determined:

$$H_\lambda \equiv \frac{\hat{\lambda}}{\hat{F}} = -\frac{1}{M_0\,\omega^2}\Bigg/\left[\sum_m \frac{\psi_{m0}^2}{M_m\, Y_m} - \frac{1}{M_0}\left(\frac{1}{\omega^2} - \frac{1}{\omega_0^2}\right)\right], \tag{A5}$$

$$H_z \equiv \frac{\hat{z}}{\hat{F}} = \frac{\hat{z}}{\hat{\lambda}}\frac{\hat{\lambda}}{\hat{F}} = \frac{1}{M_0\,\omega_0^2}\,H_\lambda, \tag{A6}$$

$$H_{z0} \equiv \frac{\hat{z}_0}{\hat{F}} = \frac{\hat{z}_0}{\hat{\lambda}} \frac{\hat{\lambda}}{\hat{F}} = \frac{H_\lambda}{M_0} \left(\frac{1}{\omega^2} - \frac{1}{\omega_0^2} \right) - \frac{1}{M_0 \omega^2}, \tag{A7}$$

$$H_{z+z0} \equiv \frac{\hat{z} + \hat{z}_0}{\hat{F}} = \frac{\hat{z} + \hat{z}_0}{\hat{\lambda}} \frac{\hat{\lambda}}{\hat{F}} = \frac{1}{M_0 \omega^2} (H_\lambda - 1). \tag{A8}$$

Following equations (21), (23) and $\omega = \omega_M$, equation (A5) may be written as

$$H_\lambda (\omega_M) = -j \Bigg/ \left\{ \frac{2M_0 \omega_M^4 \zeta_M}{M_p} \left[\sum_m \frac{\psi_{m0}^2}{\langle \psi_m^2 \rangle (\omega_m^2 - \omega_M^2)} + \frac{M_p}{M_0 \omega_M^4} \right] \right\} \tag{A9}$$

and

$$|H_\lambda (\omega_M)|^2 = \frac{s_1}{4\omega_M^4 \zeta_M^2 [s_2 + M_p / M_0 \omega_M^4]^2}, \tag{A10}$$

where

$$s_1 \equiv \left(\frac{M_p}{M_0 \omega_M^2} \right)^2, \qquad s_2 \equiv \sum_m \frac{\psi_{m0}^2}{\langle \psi_m^2 \rangle [\omega_m^2 - \omega_M^2]^2}, \tag{A11, A12}$$

$$|H_z (\omega_M)|^2 = \frac{1}{M_0^2 \omega_0^4} |H_\lambda (\omega_M)|^2, \tag{A13}$$

$$|H_{z0} (\omega_M)|^2 = \frac{1}{M_0^2 \omega_M^4} + \frac{1}{M_0^2 \omega_M^4} \left(1 - \frac{\omega_M^2}{\omega_0^2} \right)^2 |H_\lambda (\omega_M)|^2, \tag{A14}$$

$$|H_{z+z0} (\omega_M)|^2 = \frac{1}{M_0^2 \omega_M^4} (|H_\lambda (\omega_M)|^2 + 1). \tag{A15}$$

Using equations (20a–c),

$$\overline{z^2} = \frac{\pi}{4} \sum_M \frac{\omega_M^4}{\omega_0^4} \frac{\Phi_F (\omega_M)}{M_p^2 \omega_M^3 \zeta_M} g(\omega_M), \tag{A16}$$

$$\overline{z_0^2} = \frac{\pi}{4} \sum_M \frac{\Phi_F (\omega_M)}{M_p^2 \omega_M^3 \zeta_M} \left[4 \left(\frac{M_p}{M_0} \right)^2 \zeta_M^2 + \left(1 - \frac{\omega_M^2}{\omega_0^2} \right)^2 g(\omega_M) \right], \tag{A17}$$

$$\overline{(z + z_0)^2} = \frac{\pi}{4} \sum_M \frac{\Phi_F (\omega_M)}{M_p^2 \omega_M^3 \zeta_M} \left[4 \left(\frac{M_p}{M_0} \right)^2 \zeta_M^2 + g(\omega_M) \right]. \tag{A18}$$

Also, using the usual small damping assumption, $\zeta_M^2 \to 0$,

$$\overline{z_0^2} = \frac{\pi}{4} \sum_M \left(1 - \frac{\omega_M^2}{\omega_0^2} \right)^2 \frac{\Phi_F (\omega_M)}{M_p^2 \omega_M^3 \zeta_M} g(\omega_M), \tag{A19}$$

$$\overline{(z + z_0)^2} = \frac{\pi}{4} \sum_M \frac{\Phi_F (\omega_M)}{M_p^2 \omega_M^3 \zeta_M} g(\omega_M), \tag{A20}$$

where

$$g(\omega_M) = \left(\frac{M_p}{M_0\,\omega_M^2}\right)^2 \frac{s_1}{[s_2 + M_p/M_0\,\omega_M^4]^2}. \tag{A21}$$

The expression for $g(\omega_M)$ may be rewritten [5] using

$$\omega_M^4 s_2 \cong \frac{\pi^2 M^2}{4} + \left(\frac{M_p}{M_0}\right)^2,$$

and

$$\lambda_p^2 M = \pi A_p.$$

Finally then,

$$g(\omega_M) = \frac{(2m_p\,\lambda_p^2/M_0\,\pi^2)^4}{[1 + (2m_p\,\lambda_p^2/M_0\,\pi^2)^2]^2} \frac{1}{[1 + \mu_m]^2}, \tag{A22}$$

where $\mu_m = (M_p/M_0)/[(\pi^4/4)\,(A_p^2/\lambda_p^4) + (M_p/M_0)^2]$, and this term can usually be neglected.

Note that the definitions of s_1 and hence $g(\omega_M)$ in this appendix differ from those for the case where the plate is directly excited as discussed in the main text.

APPENDIX B: NOMENCLATURE

a_m	mth generalized co-ordinate with no spring/mass/damper attached
A_p	plate area
b_M	Mth generalized co-ordinate with spring/mass/damper attached
C_M	constant independent of frequency, ω, see equation (16)
F	random force
H_z	transfer function between the mass displacement, z, and external force, F
H_{z0}	transfer function between the inertial displacement, z_0, and external force, F
H_{z+z0}	transfer function between the displacement, $z + z_0$, and external force, F
M	mode number
M_0	attached mass
M_m	mth generalized mass of a plate with no spring/mass/damper attached
M_p	total plate mass
m_p	plate mass per area
w	plate deflection
z	displacement of the attached mass relative to the plate
z_0	inertial displacement of the spring end at its point of connection with plate
ω	excitation frequency
ω_0	natural frequency of spring/mass system
Ω	non-dimensional frequency
Ω_0	non-dimensional natural frequency of spring/mass system
ω_c	centre frequency
ω_m	mth modal frequency of plate with no spring/mass/damper attached
ω_M	Mth modal frequency of plate with spring/mass/damper attached
ζ_c	modal damping corresponding to ω_c
ζ_m	mth modal damping of plate with no spring/mass/damper attached
ζ_M	Mth modal damping of plate with spring/mass/damper attached
ψ_m	mth mode function of plate with no spring/mass/damper attached
ϕ_M	Mth mode function of plate with spring/mass/damper attached
Φ_z	power spectral density of the mass displacement, z
Φ_F	power spectral density of the random force, F
λ	Lagrange multiplier

λ_c average wavelength of the plate in $\Delta\omega$
λ_p wavelength of a high frequency plate mode
ΔM number of modes in the non-dimensional frequency interval
$\Delta\omega$ frequency interval
$\Delta\Omega$ non-dimensional frequency interval, $\hat{F}$, $\hat{z}$
w, $\hat{\lambda}$ amplitudes when F, z, w, λ are simple harmonic motions
$\hat{a}_m$, $\hat{b}_M$ amplitudes when a_m, b_M are simple harmonic motions
$\overline{(\cdots)^2}$ mean-square response
$\langle \cdots \rangle$ spatial average